Shielding Development for Nuclear Thermal Propulsion

Jarvis A. Caffrey[1,2], Carlos F. Gomez[2], Luke L. Scharber[2]

[1]*Department of Nuclear Engineering & Radiation Health Physics, Oregon State University, Corvallis, OR 97301*
[2]*NASA Marshall Space Flight Center, Huntsville, AL 35812*
541-227-4295; jarvis.a.caffrey@nasa.gov

Abstract. Radiation shielding analysis and development for the Nuclear Cryogenic Propulsion Stage (NCPS) effort is currently in progress and preliminary results have enabled consideration for critical interfaces in the reactor and propulsion stage systems. Early analyses have highlighted a number of engineering constraints, challenges, and possible mitigating solutions. Performance constraints include permissible crew dose rates (shared with expected cosmic ray dose), radiation heating flux into cryogenic propellant, and material radiation damage in critical components. Design strategies in staging can serve to reduce radiation scatter and enhance the effectiveness of inherent shielding within the spacecraft while minimizing the required mass of shielding in the reactor system. Within the reactor system, shield design is further constrained by the need for active cooling with minimal radiation streaming through flow channels. Material selection and thermal design must maximize the reliability of the shield to survive the extreme environment through a long duration mission with multiple engine restarts. A discussion of these challenges and relevant design strategies are provided for the mitigation of radiation in nuclear thermal propulsion.

Keywords: NTP, shielding, radiation, dose, heating

INTRODUCTION

Nuclear thermal propulsion (NTP) systems provide a dramatic improvement in performance for missions requiring both high thrust and high specific impulse, namely long duration crewed exploration missions. NTP systems can increase cargo capacity and reduce the time spent in extraplanetary space, both of which will serve to reduce overall mission risk and cosmic radiation exposure. However, NTP systems present a number of additional challenges beyond those of non-nuclear propulsion, including the need to mitigate radiation generated by nuclear fission. The growing concern of long duration exposure to cosmic radiation has now brought a great deal of focus on mitigating radiation risk in crew compartment design and material selection. In light of this growing concern for a crewed Mars mission, it is now pertinent to re-approach the problem of shielding and radiation mitigation for a nuclear thermal propulsion stage.

SHIELDING CHALLENGES

Reactor shield design should, for any reactor, be intimately involved in system design from its earliest stages. Penetrating radiation tends to produce system interfaces in otherwise unrelated components. Beyond the obvious health protective requirements, radiation shields serve vital roles to minimize unwanted radiation heating and reduce degradation of electronic and mechanical components. The process of absorbing radiation energy yields heat that must be managed in some fashion, and the shields must be able to perform reliably in the face of thermal stress and high levels of radiation exposure.

Performances Requirements

Radiation shields must be designed to meet some given performance requirement. In terrestrial reactors, this is often defined by the need to minimize the ambient dose rate at a given location or the need to minimize radiation damage

to the reactor pressure vessel. In the case of nuclear thermal propulsion there are three possible limiting requirements for a shield design. First, and most obvious, is the desire to minimize radiation dose to the crew. Second, heating in the propellant must be minimized to avoid localized boiling and pump cavitation during engine operation. Third, material damage to critical components must be held within their rated exposure limits.

Dose to Crew

Health physicists apply the principle of ALARA, or As Low As Reasonably Achievable, in common practice. An emphasis is often given to the 'Reasonable' aspect of this approach, where the benefits of lower doses must be balanced against other factors such as cost, weight, and complexity. Likewise, radiation dose to personnel in or near a nuclear propelled spacecraft should be minimized to the greatest extent possible, within reason. It must be held in perspective that the doses received by astronauts on a long term expedition outside of Earth's protective magnetic field, while still largely unknown, could certainly exceed a full Sievert (Sv) (recall that 1 Sv = 100 rem) over the course of a mission due to the pervasive galactic cosmic rays (GCR) and sporadic solar particle events (SPE). Even rudimentary shielding of a nuclear engine, combined with the inherent shielding provided by the spacecraft and cargo, would likely reduce accumulated reactor-produced dose levels to an order of magnitude less than the space radiation dose.

In any case, crew dose limits for space exploration missions are not yet fully defined, however a set of guidelines for short term and deterministic effects (Table 1) and long term stochastic effects (Table 2) were recently provided in a NASA Standard [1].

TABLE 1. Dose limits for Short-Term or Career Non-Cancer Effects (in mGy-Eq. or mGy) [2]

Organ	30-day limit	1-year limit	Career
Lens	1,000 mGy-Eq	2,000 mGy-Eq	4,000 mGy-Eq
Skin	1,500	3,000	6,000
BFO	250	500	Not applicable
Circulatory system	250	500	1000
CNS	500 mGy	1,000 mGy	1,500 mGy
CNS ($Z \geq 10$)	-	100 mGy	250 mGy

TABLE 2. Example effective dose limits for 1-year missions resulting in 3% REID, assuming equal organ dose equivalent for all tissues and no prior occupational radiation exposure [3]

	Females		Males	
Age (yr)	Avg US Adult Population	Never-Smoker	Avg US Adult Population	Never-Smokers
30	0.44 Sv	0.60 Sv	0.63 Sv	0.78 Sv
40	0.48 Sv	0.70 Sv	0.70 Sv	0.88 Sv
50	0.54 Sv	0.82 Sv	0.77 Sv	1.00 Sv
60	0.64 Sv	0.98 Sv	0.90 Sv	1.17 Sv

Such limits, when fully defined, will be based upon the combined effects of natural and manmade sources. Limits to radiation exposure from a nuclear engine will then need to be balanced against the anticipated dose received from cosmic rays. In terms of shielding efficiency, then, it makes better sense to allocate mass into combined shielding strategies within the crew compartment that can also serve to minimize dose from solar particles and secondary radiation produced from GCR collisions in the spacecraft. Concepts such as reconfigurable water bladders, food pantries, and waste storage can serve as slab shielding to mitigate radiation from the engines during their short periods of operation and then repurposed into 4π shielding during the long coasting stages where cosmic radiation burdens dominate. This principle does have limitations, however, in that high-Z materials such as lead or tungsten should not be placed near the crew compartment due to the increased production rate of secondary particles produced by GCR spallation.

Heating in Propellant

Current mission architectures for nuclear thermal propulsion feature cryogenic liquid hydrogen as a propellant due to its low atomic mass that affords the highest possible specific impulse with NERVA-type solid core designs. Liquid hydrogen also serves as a reasonably effective neutron shield, although its low density mandates extremely large storage capacities. Liquid hydrogen must be actively maintained at cryogenic temperatures as heating due to sunlight and cosmic radiation results in boil-off and requires venting to avoid excess pressurization. Absorption of nuclear

radiation energy dramatically increases the heating rate within cryogenic propellant, particularly during engine operation. As a simplified example case, consider an unshielded reactor adjacent to a cryogenic storage tank of very large diameter that imposes a geometry factor of one fifth of the 4π solid angle for isotropically emitting radiation. For a reactor operating at 1,000 MW with 0.5 percent of energy leaking by penetrating radiation, the tank will absorb about a full megawatt of thermal energy through nuclear radiation alone. Obviously, even in the absence of a crew or radiation sensitive equipment, shielding is needed to minimize this thermal burden in cryogenic storage.

Heating of cryogenic fluid during engine operation is not necessarily undesirable, though. The process of pumping fluid from the storage tank requires that the void space, or ullage, in the tank must be repressurized to maintain a constant pressure at the pump feed line. Likewise, adding thermal energy to the cryogenic fluid will not necessarily increase the system temperature, as the reducing tank pressure caused by pumping will force vaporization accompanied by cooling. From a bulk fluid perspective, then, there is a balance that may be struck between the influx of radiation energy and evaporative cooling due to pumping. In reality, though, most of the radiation is absorbed closest to the reactor. This is particularly the case for neutrons that deposit the majority of their energy within the first centimeters of liquid hydrogen at the aft tank face. The problem, then, is the effect of localized heating in the location likely to be nearest the pump inlet. The resulting effects of localized boiling and pump cavitation would lead to catastrophic failure of the turbopumps. Preventing cavitation will likely be the dominating performance requirement of a reactor shield, and establishment of radiation flux limits in this regard is ongoing.

Material Radiation Damage

Some components in a nuclear propulsion system may be sensitive to radiation damage, particularly in the case of electronic control circuits and motorized actuators. Extensive work in the field of radiation hardening for aerospace applications (electronics) and terrestrial nuclear applications (pumps, valves, and motors) will provide a wealth of options for system design. It is unlikely, then, that component radiation damage will be the largest driving factor for radiation shield design. Sensitive electronics and other components can be placed within the protection of an existing shield or utilize spot-shielding as needed. A likely candidate for the most sensitive critical component that must be reactor-adjacent is the control drum actuator stepper motor, which will likely need to incorporate an extended coupling shaft that penetrates a layer of shielding.

Thermal Performance

Radiation shielding located near an operating reactor core will be subjected to a substantial thermal load as radiation energy is converted to heat. The shielding system must maintain temperatures within acceptable limits to maintain structural integrity. In the case of a high power reactor, active cooling is required to counteract this heat generation. If active cooling is provided by coolant flow within the shield, then radiation streaming through those flow channels must be mitigated. Of particular concern is the spatially non-uniform heat generation within the shield, in which those regions closest to the core centerline are subject to heating that is several orders of magnitude greater than elsewhere in the shield.

SHIELDING DESCRIPTION

The radiation shield system for a nuclear thermal engine needs only to shield the fraction of radiation emitted toward the vehicle and crew. This ‘shadow shielding’ method is possible because of the placement of the engines at the aft of the spacecraft and lack of atmosphere or other matter to facilitate scatter. The shield must be capable of attenuating the substantial source of penetrating gamma rays emitted during engine operation, and, to a lesser extent, the continued emission of gammas from fission product decay and activation. Leakage of neutrons from the core during operation must also be mitigated, particularly for fast neutrons that must be slowed and absorbed.

Neutron shielding

Neutron shielding typically occurs in multiple stages from the perspective of individual neutrons. First, in the case of a high energy neutron, the kinetic energy must be shed by nuclear collisions. Elastic collisions with heavy nuclei such as lead or tungsten will have little effect on the kinetic energy of the incident neutron due to the conservation of momentum (think of a ping pong ball against a bowling ball). Kinetic energy is more effectively shed by collisions with lighter atoms such as carbon, beryllium, and especially hydrogen. With each scattering collision, the neutron sheds more energy and subsequently increases the chance of absorption in a receptive nucleus. The probability of

absorption is typically highest for the lowest energy neutrons, or 'thermal' neutrons in energy equilibrium with the thermal motion of their surrounding atoms. A purely elastic scattering shield, such as beryllium, is not considered effective as the thermal neutrons will exit the shield and be absorbed elsewhere. Thus, the neutron shield needs to both slow and capture the incident neutron flux. Inclusion of nuclides with a high absorption cross section is desirable, but neutron capture typically produces some form of secondary radiation emission. Shields that use absorbers producing high energy gammas must therefore account for a third stage in the neutron shielding process by absorbing these penetrating secondary photons.

Gamma shielding

Gamma shielding is, by comparison, a much simpler task. Gammas are scattered and absorbed through electron interactions, and are best attenuated by materials with a high charge density (high-Z) such as lead, tungsten, or uranium. In the case of a combined shield in which secondary gammas are produced within the neutron shield, it may seem more efficient to place all of the neutron shield material between the reactor source and the gamma shield so that fission and secondary gammas are all captured in a single layer. This would be true in the case of one-dimensional slabs where the diameter of all shield layers is constant. In a shadow-shield, however, the diameter of the shield is roughly defined by a conical solid angle of a sphere with its origin in the reactor core (in fact, the origin of that sphere would be defined by a distribution extending below the core). The consequence of this geometry is that shield layers further from the source will have a greater diameter and mass.

Material Selection

Early development in the NERVA program featured a substantial effort in material selection in which a large number of candidate materials were considered, particularly with regard to neutron shielding [4]. Of these, only a handful can be considered viable, and two such materials consistently stand out: lithium hydride and boron carbide. Comparisons of these materials could be made at great length, but for the purposes of this paper are summarized briefly.

Lithium hydride (LiH) stands out as the most effective neutron shield material per unit mass, owing to its incorporation of hydrogen as a moderator and as an excellent neutron absorber when enriched in Li-6. Its performance suffers in high-flux environments, however, as its poor thermal conductivity and narrow range of operating temperature make effective cooling strategies nearly impossible. Its reactive nature mandates that it be sealed within some containment, but its large volume expansion in melted liquid phase must be accounted for during casting and after containment closure.

Boron carbide (B_4C) stands out often as the most effective neutron shield per unit volume, but with a mass penalty in the neutron shield of about 20% greater than that of a practical lithium hydride shield. As a ceramic, B_4C has excellent thermal conductivity, hardness, and chemical stability. Although its moderating capacity is reduced by the absence of hydrogen, it does still moderate effectively and absorbs with minimal production of secondary gammas. It is currently manufactured in large quantities at relatively low cost, and although use of enriched boron-10 would increase cost above that of off-the-shelf products, those manufacturing processes would remain unchanged and are readily available.

SHIELDING ANALYSIS

Shielding design is expected to be a highly iterative process that cycles between efforts in optimizing physical effects in radiation transport and thermal performance while aiming to minimize system mass. Outer iterations in system and stage design will inevitably introduce changes to both the source term within the reactor and to performance constraints such as permissible flux. With that in mind, the best approach is to push forth with a limited set of design constraints and focus upon developing an efficient and repeatable analysis approach. The current state of shielding analysis represents a first pass at this process and the results presented herein are generally derived from non-optimized shielding designs. The processes and tools described will then be implemented within a generalized shield analysis toolkit that will enable rapid optimization based upon constraints fed by reactor design and staging parameters.

Monte Carlo Radiation Transport

Most results reported here are derived out of Monte Carlo radiation transport calculations in the MCNP6.1 transport code from Los Alamos National Laboratory (LANL) and available through the Radiation Safety Information Computational Center (RSICC) [5]. Source terms were generated in an MCNP6 model of a low-enriched reactor core

design featuring tungsten composite fuel and a large fraction of moderating tie-tubes. A broad discussion of techniques relevant to dose and shielding calculations in MCNP are provided in Kiedrowski's criticality alarm primer [6].

Source Normalization

Simulation of reactor criticality in MCNP does not explicitly behave as it would in a true reactor, particularly in terms of treatments for time and power generation. Tally measurements are normalized per neutron generated in the simulation. In order to normalize any results from a simulation to a physical unit of reactor power, the user must determine a normalization constant *C* that relates the average number of neutrons produced in the reactor per fission, $\bar{\nu}$, to the average energy produced per fission, Q, as in Equation (1).

$$C = \frac{\bar{\nu}}{Q} \tag{1}$$

It is important to note that that these values may change depending upon fuel selection, neutron energy spectra, core life cycle, and time of reactor operation. In practice, this would be calculated with conversion factors to directly relate the neutron production rate to reactor power in terms of wattage over a given time interval, with an example given in Equation (2).

$$1\,W \cdot s \left(\frac{1\ J/s}{1W}\right)\left(\frac{1\ MeV}{1.6E-13J}\right)\left(\frac{1\ Fission}{\sim 200\ MeV}\right)\left(\frac{2.445\ neutrons}{1\ Fission}\right) = 7.64E10\,\frac{n}{W \cdot s} \tag{2}$$

Surface Source Recording

MCNP permits the recording of fully characterized radiation tracks passing through a defined surface or produced within a given cell. The user can apply this 'Surface Source Write' (SSW) functionality within a criticality calculation to capture the particle fluence exiting the reactor boundaries. With careful consideration, subsequent calculations can utilize the 'Surface Source Read' (SSR) functionality to recreate the same radiation environment around the reactor with no need to track the dense population of neutrons within the core. The internal radiation environment would not be expected to change significantly between shielding design iterations, so the SSW/SSR functionality provides orders of magnitude in time savings for shielding design analysis.

Variance Reduction

Reactor shielding problems are notoriously difficult to perform in Monte Carlo analysis. The nature of a successful shield means that the total number of particles exiting the shield system is vastly lower than those entering the system, typically by many orders of magnitude. This means that out of all of the particle histories followed by the computer code, only an extremely small fraction will contribute to the scoring tallies of interest. In order to achieve reasonable statistics within those tallies, either an astronomical number of total histories must be run, or some form of variance reduction must be applied to the system. A number of such techniques were applied in these analyses, including cell importance weighting, weight windows, energy splitting, and DXTRAN, although not all concurrently. A full description of variance reduction techniques is well outside the scope of this paper, but interested readers are encouraged to consult the MCNP user's manual [7].

Time Dependent Dose Calculation

Dose rates at the crew compartment vary continuously over the duration of the mission, either through loss of shielding afforded by propellant while the engine is in operation or through the decay of fission products after engine shutdown. The time dependent behavior of dose rates in a nuclear propulsion system are of vital concern, particularly as the propellant is drained near the end of the final burn and dose rates reach a maximum before final engine cutoff. Time dependent dose rates have been modelled in MCNP by varying the propellant load within tanks of the anticipated size and shape for the current reference Mars mission profile. As could be expected, dose rates follow an exponentially increasing curve as the effective shielding thickness of propellant decreases. Gamma dose rates deviate from this trend only at points associated with the transition between stage tanks, where the geometry of the tank ends modifies the rate of change for effective shield thickness under constant flow rate conditions as seen in Figure (1a). The system can be modeled with reasonable accuracy by applying an empirical exponential function in which the dose rate is a function of remaining propellant. Alternatively, a logarithmic interpolation between the data points from the MCNP analysis can help to refine a solution.

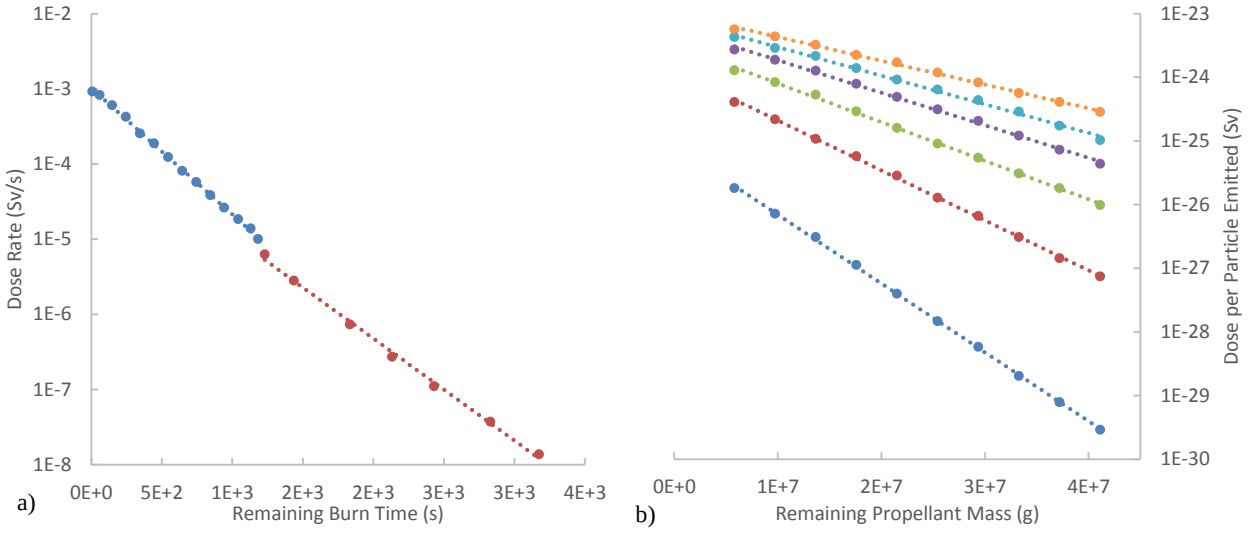

FIGURE 1. (a) Prompt dose rate during engine operation as a function of remaining burn time. (b) Dose per emitted particle for gamma rays of varying energy groups generated within the reactor core as a function of remaining propellant mass. The abscissae can be considered interchangeable, related by the total mass flow rate of propellant during operation.

Contributions to dose from delayed gammas due to buildup and decay of fission products are rather more complex and require a different approach. In one such approach, instantaneous dose rates are calculated for each of six energy groups introduced as a fixed source into the core based upon the power profile determined from analysis of the criticality run. Dose contributions are then determined per emitted particle within a series of photon energy groups. Equation (3) is used to determine energy emission rate by a set of N_j multi-exponential empirical formulas for each energy group j with varying production coefficients α_{ij} and accompanying effective half-lives λ_{ij}, based upon the reactor operating time t_o and subsequent shutdown time t_s assuming a constant fission rate P_o , the behavior of which is shown in Figure (2) [8,9,10].

$$\Gamma_j(t_o, t_s) = P_o \sum_{i=1}^{N_j} \frac{\alpha_{ij}}{\lambda_{ij}} e^{-\lambda_{ij} t_s} [1 - e^{-\lambda_{ij} t_o}] \tag{3}$$

Thus, a set of six delayed gamma terms and one fission term are used to create a series of expected instantaneous dose rate contributions at discrete propellant loads. These seven terms are combined within a purpose-built MATLAB code to analyze the dose rate throughout the mission, as shown in Figure (3). The simplified model of operation uses two conditions for calculation at discretized time steps. In the 'Engines On' condition, propellant is expended and all instantaneous dose rate components increase as the effective thickness of propellant shielding is eliminated. The fission source term is applied throughout this condition, and buildup of delayed gamma sources from fission products is added as an independent source term. In the 'Engines Off' condition, the fission source is turned off and propellant load is assumed to be static while the delayed gamma term ceases buildup and the existing inventory decays for the remainder of the calculation. Subsequent engine cycles repeat this process and all delayed gamma terms are added to the inventory built-in during the preceding runs. In the current model, no accounting is included for engine transients (startup and shutdown) and no consideration is made for absorption in fission products or bremsstrahlung from beta decay.

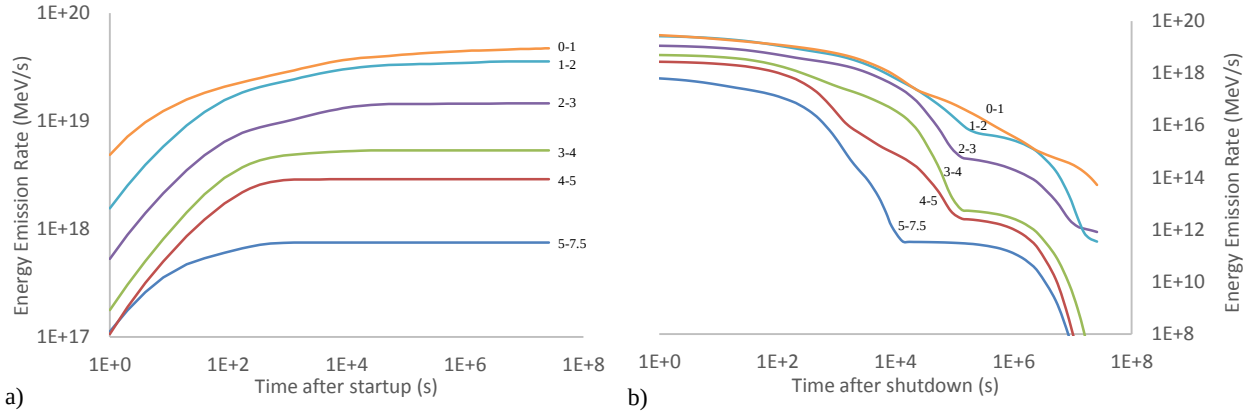

FIGURE 2. (a) Energy emission rate of fission products across 6 energy groups (labeled in MeV) building in during steady state operation at 560 MW. (b) Energy emission rate of fission products decaying after one hour of operation at 560 MW.

The upcoming model will instead use the CINDER-90 algorithm included within MCNP6 to track decay of fission and activation products. Tallies must then be discretized in time, with the resulting time-dependent distribution representing the energy release and absorption behavior after a single fission event. Further processing then yields the relevant values needed to account for source buildup and decay based upon reactor power history. Either of these methods permits flexible integration over user-defined time intervals to determine accumulated dose.

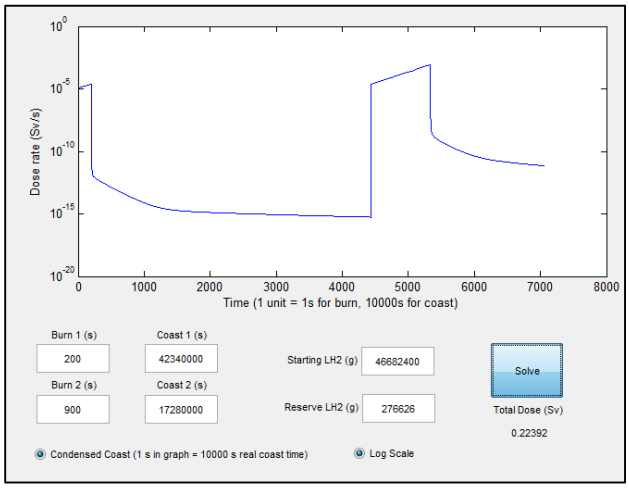

FIGURE 3. Example dose rate history calculated in the custom MATLAB code for a reactor operating at 560 MW with a basic LiH/Pb shield.

Isodose and Isoflux Contours

Early studies for component selection, sizing, and configuration in a nuclear propulsion system require a basic understanding of the radiation environment presented during engine operation. Contour plots of anticipated radiation levels are especially useful in these early phases to provide guidance for placement of sensitive components and enable simple trades between materials and cost factors. MCNP features a simple implementation of FMESH superimposed tallies that can produce spatial flux distributions. In core-centered analyses, an axisymmetric cylindrical tally is generated about the core centerline. Simple flux (F4-type) tallies may be used for flux measurements, as is often the case for neutrons separated by energy groups, however it is generally more desirable to represent these values in terms of their dose. Energy dependent dose-response factors are then applied as an FM multiplier using log-interpolated interaction coefficients, as in the left side of Figure (4) for photon dose to silicon [8]. Where crew dose is a concern, conversion coefficients were applied for ambient deep dose equivalent from neutrons and photons [11]. Silicon dose rate and neutron fast flux values are shown in Figure (4) for a reactor operating at 560 MW. Alternative representations may instead be normalized to dose/fluence per fission, dose rate/flux per $W \cdot s$, or integrated over the reactor power history to provide total dose/fluence.

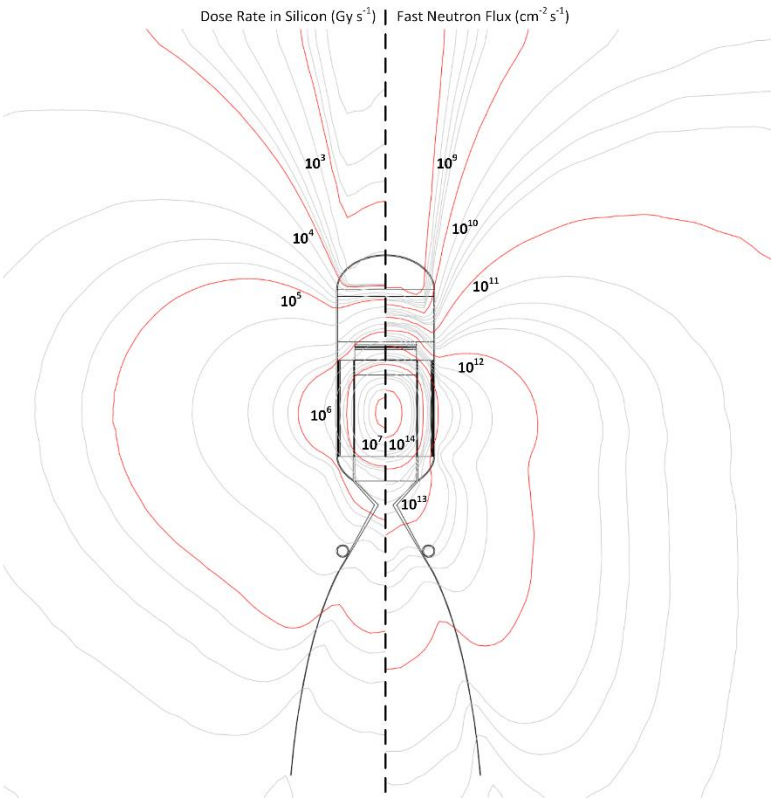

FIGURE 4. Dose rate in silicon (left) and neutron fast flux (right) profiles for a reactor operating at 560 MW with a basic LiH/Pb shield.

Thermal Analysis

Substantial heating occurs within the shield due to radiation absorption and collision processes. Bulk heating within individual cells can be calculated easily in MCNP using F6 heating tallies, which can be useful in many respects, but rigorous thermal analysis requires more detailed spatial representation of heating. Segmentation of large cells into smaller component cells is a possible solution, but such an approach is tedious and unnecessary. Instead, as in the case of dose/flux mapping, FMESH superimposed tallies can be used to resolve the spatial effects of radiation heating. An FM multiplier can be used to extract the ENDF energy dependent heating values for specified materials within a given FMESH tally. Heating mesh tallies were generated for simple representative designs featuring boron carbide neutron shield material, assumed as a pebble bed design with bulk material density adjusted to account for effective packing density. Lithium hydride was also considered earlier in the study, but brief analysis suggested that a simple cooling channel model would be inadequate to maintain sufficiently low temperatures near the reactor face and simultaneously maintain sufficiently high temperatures throughout the rest of the shield, as is needed in the case of lithium hydride. Further analysis of lithium hydride was set aside, then, in favor of advancing the more resilient boron carbide design. Lithium hydride will likely be considered in later analyses as part of a multicomponent neutron shield to mitigate fast neutron leakage, as its poor conductivity precludes its use in locations immediately adjacent to reactor components.

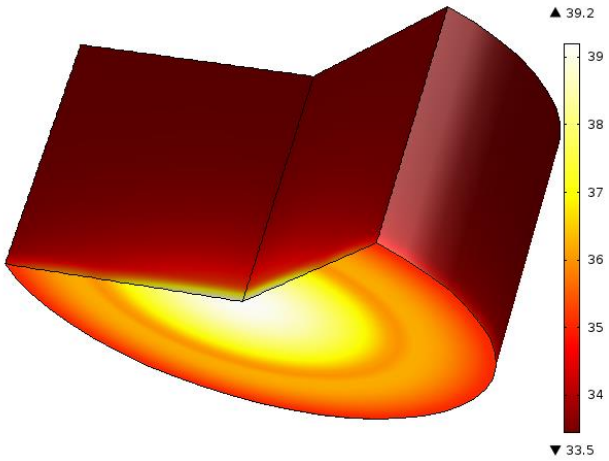

FIGURE 5. Hydrogen propellant temperature (°C) (assumed equal to pellet surface temperature) in a boron carbide pebble bed shield for a reactor operating at 560 MW after 50 seconds. Effective packing density of 0.6 assumed.

As a ceramic, boron carbide features excellent thermal conductivity and very high high temperature limits. Its hardness and chemical stability also permit more construction options. An enticing option is the use of a pebble bed design that allows generous cooling flow while minimizing radiation streaming paths. Pebble beds may also allow for ample opportunity to mix flow streams from multiple inlets prior to injection into the core. One concern for this option, however, was the magnitude of pressure drop across the shield and its negative impact on engine system power balance. That concern was abated in analysis, though, as pressure drop for a reasonable pellet diameter of 2 cm was determined to be no more than 37 kPa (5.6 psi) using the Ergun formulation as in Equation (4), and likely on the order of 15 kPa (2.2 psi) determined by Ergun formulation including the Forcheimer drag term as in Equation (5). Each equation accounts for dynamic viscosity μ, density ρ, fluid velocity V across the flow length of the shield L. In the case of Equation (5), sphere diameter D and porosity ϵ are coupled as permeability k given in Equation (6), and effects of sphere diameter on pressure drop in either case are shown in Figure (6) based upon input assumptions derived from early power balance analysis.

$$\Delta P = \frac{150\mu V_s L}{D^2}\frac{(1-\varepsilon)^2}{\varepsilon^2} + \frac{1.75\rho V^2}{D}\frac{(1-\varepsilon)}{\varepsilon^3} \tag{4}$$

$$\Delta P = \frac{\mu V_s L}{k} + \frac{1.75\rho V^2 L}{\sqrt{k}}\frac{\varepsilon}{\sqrt{150\varepsilon^3}} \tag{5}$$

$$k = \frac{D^2\varepsilon^2}{150(1-\varepsilon)^2} \tag{6}$$

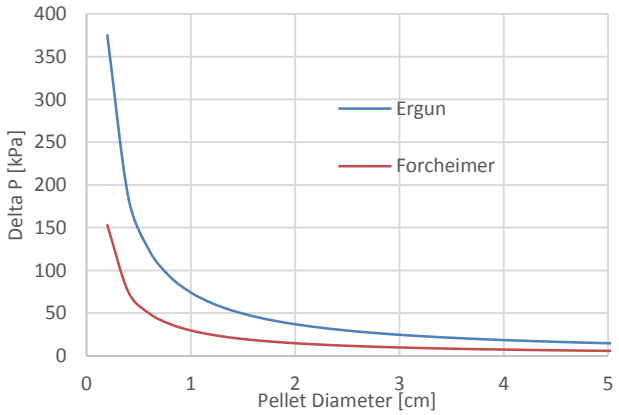

FIGURE 6. Pressure drop for gaseous hydrogen in a half-meter length pebble bed shield. Reference reactor operating at 560 MW with effective packing density of 0.6 assumed.

Mass Optimization

Given a source term and a limit for exiting radiation flux, the problem of shield optimization can be made relatively straight-forward. In the absence of such well-defined limits, the problem becomes more complex. Rather than optimizing to a single point constraint, the system must be optimized in parallel for a distribution of possible performance constraints. As an example in Figure (7), a limited set of various combinations of gamma shield thickness, neutron shield thickness, and gamma shield position are plotted in terms of total mass versus dose rate. The figure demonstrates the optimal curve, or 'Pareto front', for design variables that balance dose rate against shield mass. Points that plot farther from the optimal curve are considered dominated solutions that represent non-optimal designs. Eliminating all but those non-dominated solutions results in the 'Pareto set' of optimal solutions along the Pareto front. Selection of a point design can then be made with constrained minimization once outer constraints are established. For example, if setting a maximum terminal dose rate of 8E-13 $Sv\ s^{-1}W^{-1}$ for the scenario in Figure (7), then selecting the mass-minimized point design below that point will result in a shield mass of 1,000 kg.

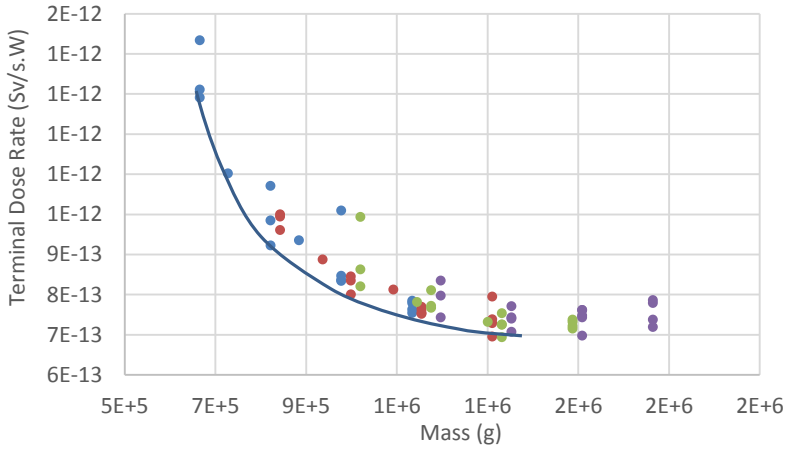

FIGURE 7. Example Pareto optimization plot for various shield designs. Points adjacent to the Pareto front represent optimal, or non-dominated, solutions.

OTHER MITIGATION STRATEGIES

Engine Placement

Standard practices of radiation protection focus upon three factors: time, distance, and shielding. In the case of a nuclear propulsion vehicle, time of exposure is already minimized by mission planning due to other inherent risks of long-duration spaceflight (including cosmic radiation exposure). Shielding is effective, but massive and costly. Distance, however, could be incorporated into a vehicle design to maximize the separation between the crew and the radiation source. For point-sources of radiation (or approximations thereof), intensity is inversely proportional to the square of distance. The current mission architecture is based upon a long-cylinder shape that houses crew opposite the engine assembly, separated by around 80 meters of propellant tanks, structure, and void space. While the length of the spacecraft may seem sufficient to minimize dose, it's important to note that a substantial portion of the radiation reaching the crew compartment is contributed by scatter in the tank assembly near the engines. Heating in propellant near the engines is also likely to be the constraining factor if it is assumed that crew will be otherwise adequately shielded against cosmic radiation.

Distancing the reactor assembly away from the bottom face of the tank benefits the system in two ways. First, the added distance reduces the unshielded radiation exposure and thus reduces the required shield thickness to meet a given flux constraint. Second, the added distance narrows the fractional solid angle extending between the source and the propellant tank face, thus reducing the required diameter of the shadow-shield and significantly reduce the required shielding mass.

A series of viable truss designs were analyzed in order to validate the feasibility of using a distance truss in place of shielding. Each design type was tested against a maximum thrust loading of 75,000 lb_f at a maximum expected gimbal

angle of 5 degrees, with lengths varying between 4 and 10 meters. For each case, the minimum required mass was determined. From this process, the most mass-efficient design was selected, shown in Figure (7a) and represented in Figure (8b), assuming construction out of Al-Mg alloy 5454. From this analysis, a polynomial expression for mass was determined as a function of length. Maximum instantaneous crew gamma dose rates were calculated at varying distances from the propellant tank using an internal shield reference design mass of approximately one metric ton.

To compare mass effectiveness of additional shielding versus that of a distance truss, a set of optimally located external disk shields of varying mass were placed between the propellant tank and engine, which was anchored at the nominal three meter distance. Figure (7b) displays the dose reduction factor, here defined as the nominal dose rate (3m, no external shield) divided over the point dose rate determined with added shield mass or with added distance in terms of truss mass.

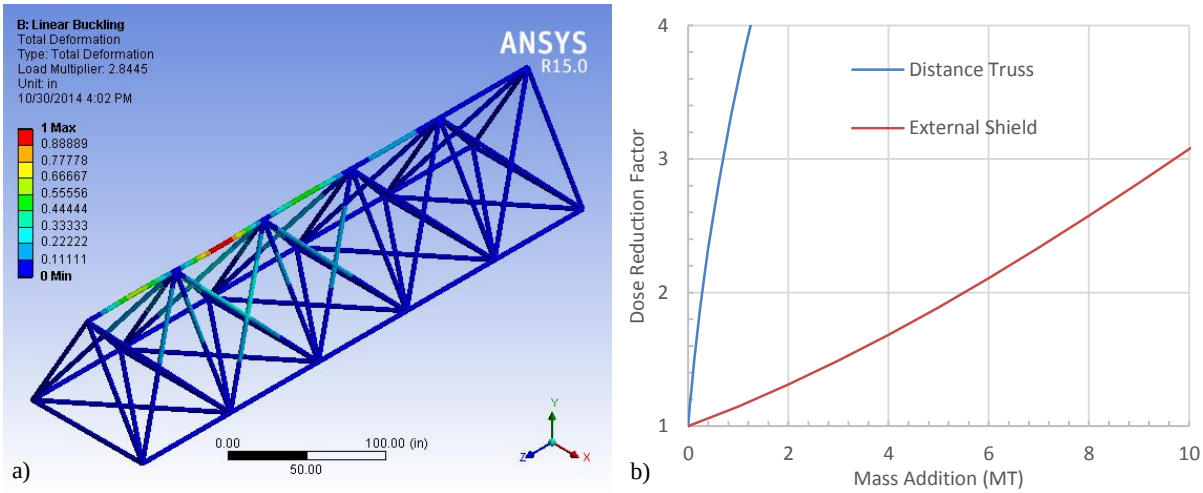

FIGURE 7. a) Buckling analysis of 10m truss determined as mass-optimal for given loading parameters. b) Comparison of gamma dose reduction factors gained by either adding

Tank and Stage Considerations

Careful planning of stage design with consideration for radiation effects will be necessary to minimize shielding mass. Earlier plans for the NERVA-powered nuclear shuttle implemented conical propellant storage tanks that minimized the exposed geometry, similar to that shown in Figure (8d). This served to reduce scatter source terms and propellant heating, and also improved terminal dose rates as the tank emptied by draining from a narrower column and thus increasing the effective thickness per unit mass of propellant acting as a shield. Some alternative considerations for mitigating dose effects and propellant heating also warrant investigation, including use of a smaller secondary tank, as in Figure (8c) with line routing schemes that prevent pump induction of heated propellant. Benefits of these design considerations must be weighed against other factors, such as cost, reliability, and payload envelope size.

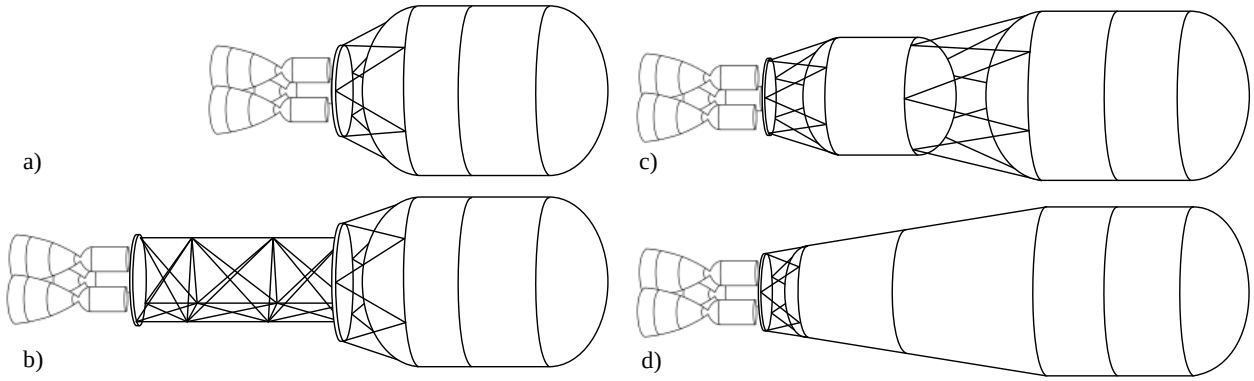

FIGURE 8. Comparison of various staging design options to mitigate radiation effects. a) Nominal core stage design. b) Distance truss. c) Thermal buffering tank. d) Conical core stage tank.

CONCLUSION

Development of radiation shielding for a nuclear thermal propulsion stage has progressed considerably in this preliminary design phase. Methods for dose and heating calculations have been refined throughout the project and continue to progress. Upcoming source terms will feature a more rigorous method of decay and activation source production using CINDER-90 production models. Thermal analysis has indicated the feasibility of implementing a pebble-bed type shield using boron carbide, and a framework has been established to quickly iterate shield designs between radiation transport and thermal analysis. Preliminary designs for a distance truss have indicated a tremendously favorable mass trade for radiation effects compared to added mass of external shielding. Boron carbide has been selected as a favorable material for neutron shielding, owing to its low cost of development and improved reliability compared to other materials. Pareto optimization techniques are in use to establish a broad range of mass-optimized shield designs, and required constraints for propellant heating to prevent cavitation and boiling are currently being developed.

ACKNOWLEDGMENTS

Special thanks are extended to Omar Mireles and Daniel Cavender of NASA Marshall Space Flight Center for their guidance in project integration, and to Wesley Deason and Michael Eades for providing interfaces with reactor design.

REFERENCES

[1] NASA Space Flight Human-System Standard Volume 1, Revision A: Crew Health (NASA-STD-3001).
[2] National Council on Radiation Protection and Measurements. Recommendations of Dose Limits for Low Earth Orbit. NCRP Report 132, Bethesda MD (2000).
[3] Cucinotta, FA, Kim, M-H, Chappell, LJ. "Space Radiation Cancer Risk Projections and Uncertainties – 2012", NASA/TP-2013-217375, (2013).
[4] Poindexter, A., Ricks, L., and Disney, R., "A Survey of Potential Shield Materials," Westinghouse Astronuclear Laboratory, WANL-TME-1345 (1966).
[5] Goorley, J.T. et al. "Initial MCNP6 Release Overview - MCNP6 Version 1.0." LA-UR-13-22934 (2013).
[6] B.C. Kiedrowski, "MCNP6 for Criticality Accident Alarm Systems -- A Primer", LA-UR-12-25545 (2012).
[7] Goorley, J.T. et al. "MCNP6 User's Manual – Version 1.0." LA-CP-13-00634 (2013).
[8] Shultis, J.K., and Faw, R.E., *Radiation Shielding*. American Nuclear Society, Inc., La Grange Park IL, (2000).
[9] George, D.C., et al., "Delayed photon sources for shielding applications," *Trans. Am. Nucl. Soc.*, **35**, 463 (1980)**.**
[10] LaBauve, R.J., England, T.R., George, D.C., Maynard, C.W., "Fission product analytic impulse source functions," *Nucl. Technol.*, **56**, 322-339 (1982).
[11] ICRP, *Conversion Coefficients for use in Radiological Protection against External Radiation*, Publication 74, International Commission on Radiological Protection, *Annals of the ICRP*, **26,** No. 3/4, Pergamon Press, Oxford, (1996).